Rotational-resonance distance measurements in multi-spin systems ☆

Aswin Verhoeven,[a] Philip T.F. Williamson,[a] Herbert Zimmermann,[b]
Matthias Ernst,[a] and Beat H. Meier[a],*

[a] *Physical Chemistry, ETH Zurich, CH-8093 Zurich, Switzerland*
[b] *Max-Planck-Institut für medizinische Forschung, Abteilung Biophysik, Jahnstrasse 29, D-69120 Heidelberg, Germany*

Abstract

It is demonstrated that internuclear distances can be evaluated from rotational-resonance (RR) experiments in uniformly ^{13}C-labelled compounds. The errors in the obtained distances are less than 10% without the need to know any parameters of the spin system except the isotropic chemical shifts of all spins. We describe the multi-spin system with a simple fictitious spin-1/2 model. The influence of the couplings to the passive spins (J and dipolar coupling) is described by an empirical constant offset from the rotational-resonance condition. Using simulated data for a three-spin system, we show that the two-spin model describes the rotational-resonance transfer curves well as long as none of the passive spins is close to a rotational-resonance condition with one of the active spins. The usability of the two-spin model is demonstrated experimentally using a sample of acetylcholine perchlorate with labelling schemes of various levels of complexity. Doubly-, triply-, and fully labelled compounds lead to strongly varying RR polarization-transfer curves but the evaluated distances using the two-spin model are identical within the expected error limits and coincide with the distance from the X-ray structure. Rotational-resonance distance measurements in fully labelled compounds allow, in particular, the measurement of weak couplings in the presence of strong couplings.
© 2004 Elsevier Inc. All rights reserved.

1. Introduction

The measurement of internuclear distances by high-resolution solid-state magic-angle spinning (MAS) NMR is an important tool for structure determination in micro-crystalline and non-crystalline samples in analogy to similar protocols available in liquid-state NMR spectroscopy [1]. Because MAS is indispensable for obtaining high spectral resolution, recoupling methods [2] must be employed to recover distance information.

Recoupling methods can be broadly divided into broadband and selective methods depending on the question whether all dipolar couplings in the sample are recovered simultaneously or whether spin pairs are recoupled selectively based on their spectral properties, e.g., the chemical shifts. Both approaches are valuable

and largely complementary, the former giving a large number of relatively inaccurate distance constraints, the latter only a few but more accurate distances. Selective methods can also be used to measure smaller dipolar couplings, corresponding to larger distances, in the presence of larger couplings [3,4], thereby, overcoming the problems of dipolar truncation [5].

The rotational-resonance experiment (RR) is a robust and widely applied method for selective homonuclear recoupling [6–8]. It requires the MAS frequency to match an integer submultiple of the isotropic chemical-shift difference between the two selected active spins, i.e., $n\omega_r = |\Omega_1^{iso} - \Omega_2^{iso}|$. The RR condition must be met to an accuracy prescribed by the magnitude of the active dipolar coupling [7,8]. Despite this inherent spectral selectivity of RR recoupling, most practical applications have been to spin systems where relatively isolated pairs have been introduced by selective labelling. Such chemically isolated spin pairs lead to particularly simple spin dynamics which has been extensively characterized [8]. The drawback of this procedure is the necessity of

---

preparing a number of selectively labelled samples which is expensive and time consuming.

We have recently shown experimentally and by numerical calculations that relatively accurate distance information (with a precision of a few percent) can indeed be obtained from uniformly ^{13}C-labelled compounds [3]. In principle, the RR polarization-transfer curves for small spin systems (less than 10 spins) can readily be calculated numerically [9]. However, such calculations require either pre-existing knowledge about the spin-system parameters (in particular J couplings, dipolar-coupling tensors, and chemical-shift tensor), or the fitting of these parameters. The strategy described in this publication aims at identifying conditions under which the RR curves can be fitted by a modified two-spin system (and ultimately a single fictitious spin 1/2) with the desired internuclear distance and an effective offset as the only relevant fit parameter. In this article, we expand our earlier phenomenological description [3] of the effects of the passive spins on the polarization-transfer curve and provide a theoretical basis for the reduction of a three-spin to a two-spin problem. Generalization to more spins is not difficult.

2. Theoretical description

We consider a three-spin system under MAS with one of the spin pairs on or close to rotational resonance. We call this spin pair the 'active' spin pair and denote these two spins with labels 1 and 2 (Fig. 1A). The active spin pair has dipolar and J couplings to an additional 'passive' spin 3 which is not on rotational resonance with either one of the active spins. For simplicity, we neglect the chemical-shift anisotropy and consider the following simple model Hamiltonian in the usual rotating frame:

$$\mathscr{H}(t) = \mathscr{H}_{cs}^{iso} + \mathscr{H}_{dd}(t) + \mathscr{H}_J \tag{1}$$

with the isotropic chemical-shift Hamiltonian

$$\mathscr{H}_{cs}^{iso} = \Omega_1 I_{1z} + \Omega_2 I_{2z} + \Omega_3 I_{3z}, \tag{2}$$

the J-coupling Hamiltonian

$$\mathscr{H}_J = 2\pi J_{12}\vec{I}_1 \cdot \vec{I}_2 + 2\pi J_{13}\vec{I}_1 \cdot \vec{I}_3 + 2\pi J_{23}\vec{I}_2 \cdot \vec{I}_3, \tag{3}$$

and the dipolar-coupling Hamiltonian

$$\mathscr{H}_{dd}(t) = b_{12}(t)(3I_{1z}I_{2z} - \vec{I}_1 \cdot \vec{I}_2) + b_{13}(t)$$
$$\times (3I_{1z}I_{3z} - \vec{I}_1 \cdot \vec{I}_3) + b_{23}(t)(3I_{2z}I_{3z} - \vec{I}_2 \cdot \vec{I}_3), \tag{4}$$

with

$$b_{ij}(t) = \sum_{\substack{n=-2\\n\neq0}}^{2}(b_{ij}^n e^{in\omega_r t}). \tag{5}$$

The constants b_{ij}^n are the Fourier coefficients of the dipolar coupling whose explicit form is given in Appendix A.

To obtain a time-independent Hamiltonian, we transform the time-dependent Hamiltonian of Eq. (1) into the appropriate interaction frame and invoke the secular approximation. The active spin pair is close to a rotational-resonance condition with a small offset $\delta_{12} = \Omega_2 - \Omega_1 - n_{12}\omega_r$. Spins 1 and 3 are offset by $\delta_{13} = \Omega_3 - \Omega_1 - n_{13}\omega_r$ from the nearest rotational-resonance condition and the corresponding rotational-resonance condition for the spin pair 2–3 is then given by $n_{23} = n_{13} - n_{12}$ leading to $\Omega_3 - \Omega_2 = \delta_{13} - \delta_{12} + n_{23}\omega_r$.
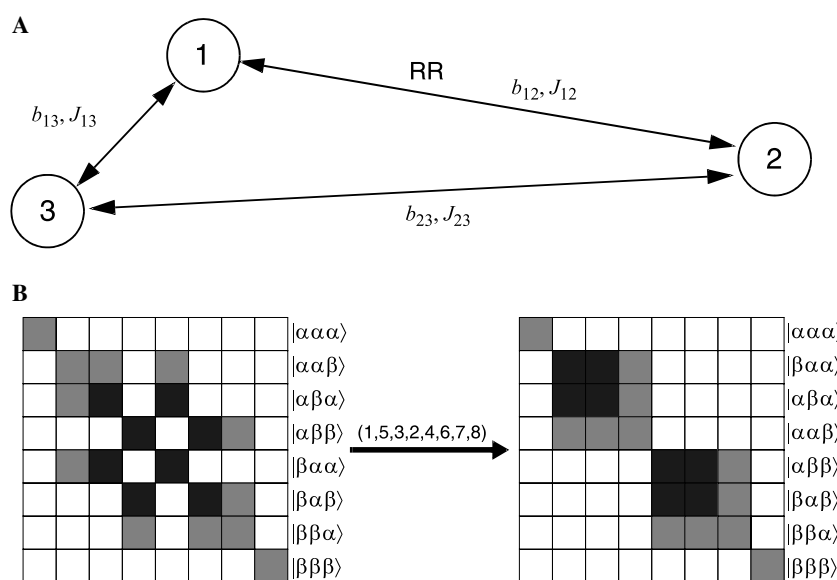

Fig. 1. (A) Topology of the spin system used in the simulations. Spins 1 and 2 form the "active" spin pair which is on rotational resonance while spin 3 is the passive spin. (B) Schematic representation of the block diagonalization of the three-spin Hamiltonian of Eq. (8). The 2 × 2 subspaces of the active spin pair are shown in black, the elements outside these subspaces in a lighter shading.

We can rewrite the isotropic chemical-shift Hamiltonian of Eq. (2) using the rotational-resonance conditions mentioned above and obtain

$$\mathscr{H}_{cs}^{iso} = \Omega_1 F_z + (n_{12}\omega_r + \delta_{12})I_{2z} + (n_{13}\omega_r + \delta_{13})I_{3z} \quad (6)$$

with the total spin operator $F_z = I_{1z} + I_{2z} + I_{3z}$. Except for the offsets from the rotational-resonance condition this Hamiltonian has the required form for the rotating-frame transformation operator, namely:

$$R = \mathscr{H}_{cs}^{iso} - (\delta_{12}I_{2z} + \delta_{13}I_{3z})$$
$$= \Omega_1 F_z + n_{12}\omega_r I_{2z} + n_{13}\omega_r I_{3z}. \quad (7)$$

Neglecting all time-dependent terms in the interaction-frame Hamiltonian, $\exp(-iRt)\mathscr{H}\exp(Rt)$, we obtain a time-independent zeroth-order average Hamiltonian

$$\overline{\mathscr{H}} = \overline{\mathscr{H}}_{cs}^{iso} + \overline{\mathscr{H}}_{dd} + \overline{\mathscr{H}}_J, \quad (8)$$

with the chemical-shift Hamiltonian

$$\overline{\mathscr{H}}_{cs}^{iso} = \delta_{12}I_{2z} + \delta_{13}I_{3z}, \quad (9)$$

the J-coupling Hamiltonian

$$\overline{\mathscr{H}}_J = 2\pi J_{12}I_{1z}I_{2z} + 2\pi J_{13}I_{1z}I_{3z} + 2\pi J_{23}I_{2z}I_{3z}, \quad (10)$$

and the dipolar-coupling Hamiltonian

$$\overline{\mathscr{H}}_{dd} = b_{12}^n\left(\tfrac{1}{2}(I_1^+ I_2^- + I_1^- I_2^+)\right) + b_{13}^n\left(\tfrac{1}{2}(I_1^+ I_3^- + I_1^- I_3^+)\right)$$
$$+ b_{23}^n\left(\tfrac{1}{2}(I_2^+ I_3^- + I_2^- I_3^+)\right). \quad (11)$$

It is well known that the matrix representation of the Hamiltonian of Eq. (8) is block diagonal if the basis functions are ordered according to the total magnetic quantum number f_z (see Fig. 1B). Because the initial density operator can also be block diagonalized in the same way, the time evolution of the spin system can be evaluated for each subspace separately. We can restrict the discussion to the two 3×3 zero-quantum (ZQ) subspaces with the matrix representation

tions $|n_{ij}| = 1, 2$ while the presence of shift anisotropy can lead to nonzero values for all integer values of n, including 0. Each ZQ subspace supports three zero-quantum transitions and the difference polarization of the two active spins $S(t) = \langle I_{1z} - I_{2z} \rangle(t)$ can be written in the general form

$$S(t) = C + A_{12}^{+1/2}\cos(\omega_{12}^{+1/2}t) + A_{13}^{+1/2}\cos(\omega_{13}^{+1/2}t)$$
$$+ A_{23}^{+1/2}\cos(\omega_{23}^{+1/2}t) + A_{12}^{-1/2}\cos(\omega_{12}^{-1/2}t)$$
$$+ A_{13}^{-1/2}\cos(\omega_{13}^{-1/2}t) + A_{23}^{-1/2}\cos(\omega_{23}^{-1/2}t). \quad (14)$$

The seven amplitudes C and $A_{ij}^{\pm1/2}$ and the six frequencies $\omega_{ij}^{\pm1/2}$ can be evaluated analytically from the matrices given above. The resulting general equations are, however, lengthy and do not provide much insight into the problem. Furthermore, they are usually not suited to analyze experimental data because of the large number of parameters that have either to be known beforehand, assumed, or fitted.

We, therefore, introduce a simple perturbation treatment which reduces the three-spin problem to an effective two-spin problem for the case that the two active spins are close to rotational resonance and the passive spins are far from any rotational-resonance condition. Reduction to an effective 2-spin system is equivalent to block-diagonalizing the two 3×3 subblocks (see Fig. 1B) into a 1×1 and a 2×2 subblock. The two 2×2 subblocks represent the fictitious spin-1/2 systems which describe, approximately, the ZQ subspace of the active spin pair. In this approximation, the two 2×2 subblocks provide all the information needed to calculate $S(t)$. In the present treatment, a single passive spin is taken into account but the generalization to a larger number of passive spins is possible. We separate the Hamiltonian into an unperturbed part $\overline{\mathscr{H}}_{\pm1/2}^{(0)}$ which contains the diagonal elements and the active dipolar coupling and into a perturbation $V_{\pm1/2}$ which contains the passive couplings and is defined

$$\overline{\mathscr{H}}_{1/2}^{ZQ} = \frac{1}{2}\begin{bmatrix} \pi(-J_{12} - J_{13} + J_{23}) + \delta_{12} + \delta_{13} & -b_{12}^n & -b_{13}^n \\ -(b_{12}^n)^* & \pi(-J_{12} + J_{13} - J_{23}) - \delta_{12} + \delta_{13} & -b_{23}^n \\ -(b_{13}^n)^* & -(b_{23}^n)^* & \pi(J_{12} - J_{13} - J_{23}) + \delta_{12} - \delta_{13} \end{bmatrix}, \quad (12)$$

and

$$\overline{\mathscr{H}}_{-1/2}^{ZQ} = \frac{1}{2}\begin{bmatrix} \pi(-J_{12} - J_{13} + J_{23}) - \delta_{12} - \delta_{13} & -(b_{12}^n)^* & -(b_{13}^n)^* \\ -b_{12}^n & \pi(-J_{12} + J_{13} - J_{23}) + \delta_{12} - \delta_{13} & -(b_{23}^n)^* \\ -b_{13}^n & -b_{23}^n & \pi(J_{12} - J_{13} - J_{23}) - \delta_{12} + \delta_{13} \end{bmatrix}. \quad (13)$$

Note that the coupling elements b_{ij}^n in the two matrices given above are the Fourier components corresponding to the n_{ij} rotational-resonance condition for the transition involved. In the absence of chemical-shift anisotropy, they are only nonzero for the four condi-

(for the +1/2 subspace) by

$$V_{1/2} = \frac{1}{2}\begin{bmatrix} 0 & 0 & -b_{13}^n \\ 0 & 0 & -b_{23}^n \\ -(b_{13}^n)^* & -(b_{23}^n)^* & 0 \end{bmatrix}. \quad (15)$$

The correction to the diagonal elements of $\overline{\mathscr{H}}^{(0)}_{1/2}$ can be obtained in second-order perturbation theory by

$$E_1^{(2)} = \frac{|b_{13}^n|^2}{4\pi(-J_{12}+J_{23})+4\delta_{13}} \cong \frac{|b_{13}^n|^2}{4\delta_{13}},$$

$$E_2^{(2)} = \frac{|b_{23}^n|^2}{4\pi(-J_{12}+J_{13})-4\delta_{12}+4\delta_{13}} \cong \frac{|b_{23}^n|^2}{4\delta_{13}}, \quad (16)$$

$$E_3^{(2)} = -E_1^{(2)} - E_2^{(2)}.$$

Neglecting the part proportional to the unity operator, the 2×2 zero-quantum subspaces of the active spin pair can now be written as

$$\overline{\mathscr{H}}_{\pm 1/2} = \Delta_{12}^{\pm 1/2} S_z^{ZQ} + |b_{12}^n| S_\varphi^{ZQ}, \quad (17)$$

with

$$\Delta_{12}^{\pm 1/2} = -\pi J_{13} + \pi J_{23} \pm \delta_{12} \pm \frac{|b_{13}^n|^2}{4\delta_{13}} \mp \frac{|b_{23}^n|^2}{4\delta_{13}}. \quad (18)$$

The operators S_z^{ZQ} and S_φ^{ZQ} are fictitious spin-1/2 operators in the 2×2 zero-quantum subspace of the active spin pair and S_φ^{ZQ} is a generalized transverse spin operator in the xy plane as defined by

$$S_\varphi^{ZQ} = \cos(\varphi) S_x^{ZQ} + \sin(\varphi) S_y^{ZQ}, \quad (19)$$

where φ depends on the phase of the complex Fourier component b_{12}^n. By a simple (crystal orientation dependent) z-rotation, the dipolar field can be aligned with the x-axis of the ZQ subspace:

$$\overline{\mathscr{H}}_{\pm 1/2} = \Delta_{12}^{\pm 1/2} S_z^{ZQ} + |b_{12}^n| S_x^{ZQ}. \quad (20)$$

Eq. (20) is formally identical to the Hamiltonian of a two-spin system under off-RR conditions. The crystal-orientation-dependent effective RR mismatch $\Delta_{12}^{\pm 1/2}$ depends on the passive dipolar and J couplings. In the absence of J couplings, the offsets in the two subblocks are the same, except of the sign and the time evolution in the two subspaces is identical. We furthermore note that in the absence of J couplings the offset $\Delta_{12}^{\pm 1/2}$ for a single crystallite, but not in the powder average, can be removed by setting the MAS frequency slightly offset ($\delta_{12} \neq 0$) from the exact RR condition.

The time evolution of the difference polarization in such a two-spin model is given by

$$\frac{S(t)}{S(0)} = \frac{1}{2}[C + A^{-1/2}\cos(\omega_{\text{eff}}^{-1/2}t) + A^{+1/2}\cos(\omega_{\text{eff}}^{+1/2}t)], \quad (21)$$

with

$$A^{\pm 1/2} = \frac{|b_{12}^n|^2}{(\omega_{\text{eff}}^{\pm 1/2})^2}, \quad C = \frac{(\Delta_{12}^{+1/2})^2}{(\omega_{\text{eff}}^{+1/2})^2} + \frac{(\Delta_{12}^{-1/2})^2}{(\omega_{\text{eff}}^{-1/2})^2},$$

$$\omega_{\text{eff}}^{\pm 1/2} = \sqrt{|b_{12}^n|^2 + (\Delta_{12}^{\pm 1/2})^2}. \quad (22)$$

The condition $|\Delta_{12}^{+1/2}| = |\Delta_{12}^{-1/2}|$ is often fulfilled to a good approximation even in the presence of J couplings

and is exact in the absence of J couplings. The well-known equations for rotational-resonance polarization transfer in an isolated two-spin system are then recovered:

$$\frac{S(t)}{S(0)} = C + A \cdot \cos(\omega_{\text{eff}}t) \quad (23)$$

with

$$C = \frac{(\Delta_{12})^2}{(\omega_{\text{eff}})^2}, \quad A = \frac{|b_{12}^n|^2}{(\omega_{\text{eff}})^2}, \quad \omega_{\text{eff}} = \sqrt{|b_{12}^n|^2 + (\Delta_{12})^2}. \quad (24)$$

Such a description of the time evolution of the difference polarization does not include relaxation. In many cases, however, the relaxation-rate constant (in the zero-quantum subspace) is in the same order of magnitude as the dipolar coupling of the active spin pair and can, therefore, not be neglected. The Liouville-space description of the time evolution, introduced by Levitt et al. [8], includes relaxation according to

$$\hat{\hat{\mathscr{L}}}_{\pm 1/2} = -\mathrm{i}\hat{\mathscr{H}}_{\pm 1/2} - \hat{\hat{\Gamma}}_{\pm 1/2}, \quad (25)$$

where the relaxation operator describes a random field along the z axis, as defined by

$$\hat{\hat{\Gamma}} = k_1[I_{1z},[I_{1z},]] + k_2[I_{2z},[I_{2z},]]. \quad (26)$$

Here, k_1 and k_2 are the transverse relaxation-rate constants of the spins 1 and 2. Assuming the random fields on the two spins are uncorrelated, they constitute an effective transverse relaxation rate in the zero-quantum subspace with $R_2 = k_1 + k_2$.

In a basis spanned by the fictitious spin-1/2 operators $(S_x^{ZQ}, S_y^{ZQ}, S_z^{ZQ})$, the matrix representation of the Liouvillian can be written as

$$\hat{\hat{\mathscr{L}}}_{12}^{\pm 1/2} = \begin{bmatrix} -R_2 & -\Delta_{12}^{\pm 1/2} & 0 \\ \Delta_{12}^{\pm 1/2} & -R_2 & -|b_{12}^n| \\ 0 & |b_{12}^n| & 0 \end{bmatrix}. \quad (27)$$

As pointed out above, the offset terms $\Delta_{12}^{\pm 1/2}$ can often be assumed to be identical and the superscript can be omitted. Under this approximation, the density operator in the zero-quantum subspace evolves according to

$$\sigma(t) = \exp(\hat{\hat{\mathscr{L}}}t)\sigma(0) \quad (28)$$

with the initial density operator, in vector representation, given by $\sigma(0) = [0, 0, S(0)]^T$. This equation is isomorphic with the Bloch equations with transverse but no longitudinal relaxation. Starting with an initial density operator proportional to S_z^{ZQ}, it leads to a damped oscillation of the difference polarization $S(t)$ with an effective frequency ω_{eff} (see Eq. (22)). The non-oscillating part (term C in Eq. (21)) will also decay to zero under the action of R_2 according to the coupled system of equations defined by the Liouvillian.

To account for a possible pedestal of signal-components not decaying under the zero-quantum relaxation

mechanism (e.g., caused by natural-abundance signals and overlap with other resonances not coupled to the active spin system), we add a phenomenological term $\sigma(\infty) = [0, 0, S(\infty)]^T$ and obtain the equation of motion

$$\sigma(t) = \exp(\hat{\hat{\mathscr{L}}}t)\sigma(0) + \sigma(\infty). \tag{29}$$

This equation will be used to describe the spin system. The observable $S(t)$ in the RR experiment is the third vector component of $\sigma(t)$. Relevant model parameters are the active dipolar coupling b_{12}^n, the offset $\Delta_{12}^{\pm 1/2}$, the zero-quantum relaxation rate constant R_2 and the phenomenological offset $S(\infty)$.

It should be noted that both the effective offset and the dipolar coupling are functions of the crystallite orientation with respect to a rotor-fixed coordinate system, i.e., $\Delta_{12}^{\pm 1/2} = \Delta_{12}^{\pm 1/2}(\alpha, \beta, \gamma)$ and $b_{12}^n = b_{12}^n(\alpha, \beta, \gamma)$. Therefore, a powder average must be performed to obtain the time evolution.

For a numerical treatment, it is also possible to avoid the secular approximation employed to obtain Eq. (8) and to keep the time-dependent components of the dipolar coupling tensors. Then a time-dependent model Liouvillian is used

$$\hat{\hat{\mathscr{L}}}_{\pm 1/2} = \begin{bmatrix} -R_2 & \mp n_{12}\omega_r - \Delta_{12}^{\pm 1/2} & 0 \\ \pm n_{12}\omega_r + \Delta_{12}^{\pm 1/2} & -R_2 & -b_{12}(t) \\ 0 & b_{12}(t) & 0 \end{bmatrix} \tag{30}$$

and the Liouville–von-Neumann equation is solved by the method of time slicing. In this case, the presence of chemical-shift anisotropy for the active spins can easily be integrated.

3. Analysis of the equations in the absence of relaxation

To obtain an estimate how well the approximate two-spin model developed in the previous chapter describes a multi-spin system, numerically exact Hilbert-space calculations of an example three-spin system were performed using the spin-simulation environment GAMMA [9]. The active spin pair was chosen to have an internuclear distance $r_{12} = 4.0\,\text{Å}$ (corresponding to the anisotropy of the dipolar coupling $\delta_D^{(1,3)} = 118.5\,\text{Hz}$) and no J coupling. All calculations were performed on the exact rotational-resonance condition of the active spin pair with $\omega_r/(2\pi) = 20\,\text{kHz}$, and $\delta_{12} = 0$. To simplify the situation the coupling between spins 2 and 3 of our model system was set to zero, i.e., $J_{23} = b_{23} = 0$. The relative orientation of the two dipolar couplings (1,2) and (1,3) was chosen to be $\beta = 90°$.

The exact simulations (Fig. 2, black lines) are compared to approximate solutions of Eqs. (23) and (24) (Fig. 2, red lines) describing an effective two-spin system and an approximate analytical description of the three-spin system in secular approximation as described in Appendix B (Fig. 2, blue lines) for four different situations: (i) For an isolated two-spin system, i.e., $J_{13} = 0\,\text{Hz}$ and $b_{13} = 0\,\text{Hz}$. The three curves are, as expected, indistinguishable showing that for the present case the secular approximation of Eq. (8) is very good; (ii) Adding a passive J coupling, $J_{13} = 50\,\text{Hz}$, which corresponds to a spin system with a heteronuclear passive spin, leads to the behaviour shown in Fig. 2B with a modified precession frequency and a pedestal which are excellently described by the two-spin model of Eq. (23); (iii) In the presence of a strong passive dipolar coupling
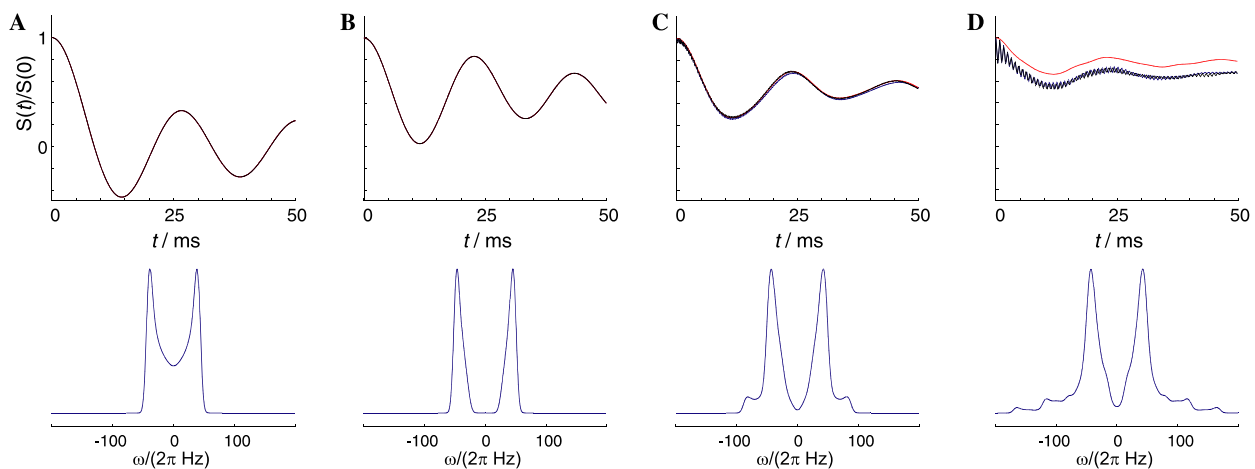

Fig. 2. Polarization-transfer curves of a powder sample calculated using Eq. (21) (red), Eq. (B.1) (blue), and by performing an exact Hilbert-space simulation of the spin system (black). For the blue curves the frequency-domain data are shown below the time-domain data. All data were calculated at exact rotational resonance for the active spin pair. In (A) the curves show a two-spin system with $r_{12} = 4.0\,\text{Å}$ and $\omega_r/(2\pi) = 20\,\text{kHz}$. In (B) a passive spin was added, with $J_{13} = 50\,\text{Hz}$ but no dipolar coupling equivalent to a situation where the passive spin pair is far from any RR condition. In (C) the passive spin is close to the $n = 1$ RR condition with spin 1, with $r_{13} = 1.5\,\text{Å}$ and $\delta_{13}/(2\pi) = 3\,\text{kHz}$. In (D) the passive spin is even closer to the $n = 1$ RR condition with spin 1, i.e., $\delta_{13}/(2\pi) = 1\,\text{kHz}$.

($\delta_D^{(1,3)} = 2248$ Hz) and a J coupling ($J_{13} = 50$ Hz) to a passive spin off rotational resonance by $\delta_{13}/(2\pi) = 3$ kHz the simple two-spin approximation (Eq. (23)) is still quite good as can be seen in Fig. 2C. However, some additional low-amplitude high-frequency oscillations become apparent which cannot be described by the pseudo two-spin model but by the additional frequencies contained in Eq. (14); (iv) If the offset from the rotational-resonance condition $\delta_{13}/(2\pi)$ is reduced further, these high-frequency oscillations become stronger. This is shown in Fig. 2D, where the offset is smaller than 1 kHz, which is less than the passive dipolar coupling. These components decrease in frequency but increase in amplitude for decreasing values of δ_{13}. The simplified model does not only fail to reproduce the high frequency oscillations, it also gives the wrong magnitude for the amplitude of the time-independent term. Despite the small offset from the rotational-resonance condition for the passive spin pair, the approximate description from Appendix B still leads to good results. The shape of the exchange curves also depends somewhat on the relative orientation of the active and passive dipolar coupling tensors (see Additional material).

Larger deviations can be observed at lower MAS frequencies. If the calculation of Fig. 2C is repeated with an MAS frequency of $\omega_r/(2\pi) = 5$ kHz, while adjusting the chemical-shift difference of the active spin pair to remain on the $n = 1$ rotational resonance, larger deviations of the approximate solution from the exact simulations are observed (Fig. 3). This is due to the fact that the spin pair 1–3 is now simultaneously close to two rotational-resonance conditions since the offset from the $n_{13} = 1$ condition is 3 kHz and the offset from the $n_{13} = 2$ condition is 2 kHz. In this case, the secular approximation, which takes into account only the

closest RR condition of the spin pair 1–3, becomes inadequate.

4. Analysis of the equations including relaxation effects

To interpret the experimental RR polarization-transfer curves from multiply labelled samples, three simple models all based on the Liouvillian of Eq. (27) were employed:

(A) In the simplest approach, the multi-spin system was treated like a two-spin system on rotational resonance and the offsets $\Delta_{12}^{\pm 1/2}$ were set to zero. A powder average was calculated using the Liouvillian of Eq. (27) with the dipolar-coupling constant b_{12} and the zero-quantum relaxation-rate constant R_2 as well as the initial polarization difference $S(0)$ as free parameters (see also Eq. (28)).

(B) Based on the observation that the dipolar oscillation is offset by a value C, the model A was extended by a pedestal for the dipolar oscillation (or a base-line offset for the transfer curves). This is the model employed in [3]. Free fit parameters are $S(0)$, b_{12}, R_2, and the pedestal $S(\infty)$ (see also Eq. (29)).

(C) The full Liouvillian of Eq. (27) with $\Delta_{12}^{\pm 1/2} \neq 0$, according to the model sketched in Chapter 2 was used in this model. Since the orientation-dependent offset from the rotational-resonance condition $\Delta_{12}^{\pm 1/2}(\alpha, \beta, \gamma)$ depends on the usually unknown relative orientation of the two dipolar-coupling tensors, the approximation $\Delta_{12}^{+1/2}(\alpha, \beta, \gamma) = \Delta_{12}^{-1/2}(\alpha, \beta, \gamma) = \bar{\Delta}$ was used, where $\bar{\Delta}$ is constant and independent of the crystal orientation. Free parameters of the fit (according to Eq. (29)) are the dipolar-coupling constant b_{12}, the zero-quantum relaxation-rate constant R_2, the initial polarization difference $S(0)$, and the average effective offset from the RR condition $\bar{\Delta}$. $S(\infty)$ was held constant at the value expected from the natural-abundance contributions.

To estimate the errors associated with the three models, we have fitted the numerically exact polarization-transfer curves for a three-spin model system with each of the three two-spin models described above. The three-spin simulations were performed in the full Liouville space using the GAMMA spin-simulation environment [9] complemented by block-diagonalization code to speed up the matrix diagonalization. Relaxation was implemented as described by Eqs. (25) and (26). The relaxation-rate constants were chosen to be identical for every spin ($k_1 = k_2 = 100\,\text{s}^{-1}$). The maximum mixing time in each simulation was chosen as a function of the distance according to $\tau_m^{max} = 5\,\text{ms} \cdot (r_{12}/(1.5\,\text{Å}))^3$ or $\tau_m^{max} = 100$ ms whichever is shorter. In this way we account for the decreasing oscillation frequency of the transfer process for longer distances. The difference polarization was sampled every rotor period. Gaussian noise with a standard deviation of 0.005 was added to
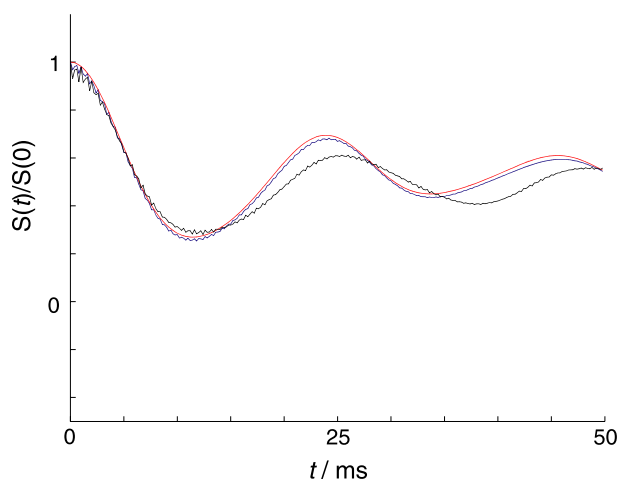

Fig. 3. Polarization transfer curves generated in a similar way as in Fig. 2. In these simulations the MAS frequency is reduced to $\omega_r/(2\pi) = 5$ kHz. The passive spin is now close to both the $n = 1$ ($\delta_{13}/(2\pi) = 3$ kHz) and the $n = 2$ ($\delta_{13}/(2\pi) = 2$ kHz) RR conditions.

Table 1
Parameters for the numerical simulations in the three-spin model

	4A–C simulations	5B simulations
$(\Omega_1$ (Hz), δ_1 (Hz), $\eta_1)$	(0, 0, 0)	(0, 6083, 0.2466)
$(\alpha_1, \beta_1, \gamma_1)$	(–, –, –)	(36°, 134°, 127°)
$(\Omega_2$ (Hz), δ_2 (Hz), $\eta_2)$	(variable, 0, 0)	(variable, 1542, 0.2432)
$(\alpha_2, \beta_2, \gamma_2)$	(–, –, –)	(160°, 137°, 82°)
$(\Omega_3$ (Hz), δ_3 (Hz), $\eta_3)$	(18750, 0, 0)	(18750, 9250, 0.8919)
$(\alpha_3, \beta_3, \gamma_3)$	(–, –, –)	(42°, 109°, 87°)
d_{12} (Hz) $(r_{12}$ (Å))	Variable	Variable
$(\alpha_{12}, \beta_{12}, \gamma_{12})$	(0°, 0°, 0°)	(0°, 0°, 0°)
d_{13} (Hz) $(r_{13}$ (Å))	2248 (1.54)	2248 (1.54)
$(\alpha_{13}, \beta_{13}, \gamma_{13})$	(0°, 109.5°, 0°)	(0°, 109.5°, 0°)
d_{23} (Hz) $(r_{23}$ (Å))	0 (∞)	0 (∞)

the curves after normalizing the first point to a value of 1. The χ^2 of the fit was normalized according to the noise, i.e., a perfect fit would result in a $\chi^2 = 1$. The parameters for the spin systems used in these simulations and fits are summarized in Table 1. The fitting program uses the optimization routines from the package MINUIT [10].

The simulated data for the three-spin system was fitted with models A, B, and C, respectively which all employ an effective two-spin system. The results of this analysis are presented in Figs. 4A–C as the relative deviation of the fitted distance from the actual distance used in the simulations. As expected, strong deviations (more than 15%) in the resulting distances are observed near the $n = 1$ and $n = 2$ rotational-resonance conditions for the passive spin, i.e., at $\Omega_3 - \Omega_1 \approx n\omega_r$ using model A (Fig. 4A). The deviations in the distance are reduced for model B (Fig. 4B) and even more so when using model C with $S(\infty) = 0$ (Fig. 4C). This is also illustrated by a general decrease in the χ^2 of the fits, as shown in Figs. 4D–F. For a large range of spin-system parameters, the fit yields the "true" distance within 10% accuracy. Regions where the fitted distance does not agree with the true distance are often (in particular for model C) but not always flagged by bad fits as expressed by large χ^2 values (compare Figs. 4A–C with D–F).

Using our simulated data, we can check the systematic errors introduced by neglecting the angular dependence of $\Delta_{12}^{\pm1/2}(\alpha, \beta, \gamma)$ and using the approximation of

an Euler-angle independent offset value $\bar{\Delta}$. We have, therefore, repeated the fit with model C with a fit by a model D which uses the dipolar-coupling constant b_{12}, the zero-quantum relaxation-rate constant R_2, and the initial polarization difference $S(0)$ as free parameters. The pedestal $S(\infty)$ is set to zero. The orientation-dependent offset from the rotational-resonance condition $\Delta_{12}^{\pm1/2}(\alpha, \beta, \gamma)$ is calculated from the spin-system data which involves knowledge of the parameters of the passive spins. The resulting fit is shown in Fig. 5A and is very similar to the one of Fig. 4C indicating that this approximation of model C is justified.

Our models ignore the effects of chemical-shift anisotropy. Formally, this additional interaction is easy to include into the theoretical description [7,8]. Since the magnitude and orientation of the chemical-shift tensors are often unknown their effects are usually ignored in the analysis at the expense of some systematic errors. The situation is similar in our case. The simulated spectra that were analyzed by our models A–C in Fig. 4 were generated without anisotropic chemical-shift interactions. Anisotropic chemical-shift terms were included in the simulations used for Fig. 5B (see Table 2) but the analysis was still performed in the framework of our simple model C ignoring chemical-shift anisotropy effects. Clearly, the inclusion of chemical-shift anisotropies in the simulated data reduces the fidelity with which internuclear distances can be determined. However, this happens primarily in an area where the MAS frequency becomes so slow that it is exceeded by the sizes of the CSA tensors. This finding is in accordance with observations on isolated two-spin systems [8].

5. Fits of experimental RR polarization-transfer curves

In the previous two sections we have illustrated by way of representative examples that the effect of the passive spins on the polarization-transfer curves can be described by an effective two-spin system. Models B and C have been shown to yield improved accuracy compared to simply neglecting the passive spins (model A). In the following we use models B and C to analyze the experimental RR polarization-transfer curves of four differently labelled acetylcholine perchlorate samples representing chemically isolated two-spin, three-spin, or

Fig. 4. Relative difference between the true internuclear distance of the active spin pair in a three spin system and the value obtained by a least square analysis using: (A) model A, (B) model B, and (C) model C as described in the text. The plots are given as a function of the internuclear distance of the active spins r_{12} and the chemical-shift difference of the active spins $\Omega_1 - \Omega_2$. The chemical-shift difference between the active and the passive spins was kept constant at $(\Omega_3 - \Omega_1)/(2\pi) = 18.75$ kHz. The MAS frequency ω_r was set to $\Omega_1 - \Omega_2$ in order to always fulfill the RR condition for the active spin pair. (D–F) show the least square deviations of the simulated data and the best fit by models A–C.

Fig. 5. (A) Relative difference between the true internuclear distance between the active spins in a three-spin system and the value obtained by a least-square analysis using model D described in the text. (B) Analysis of a simulated three-spin spectrum including chemical-shift anisotropy (see Table 1) by model C as described in the text.
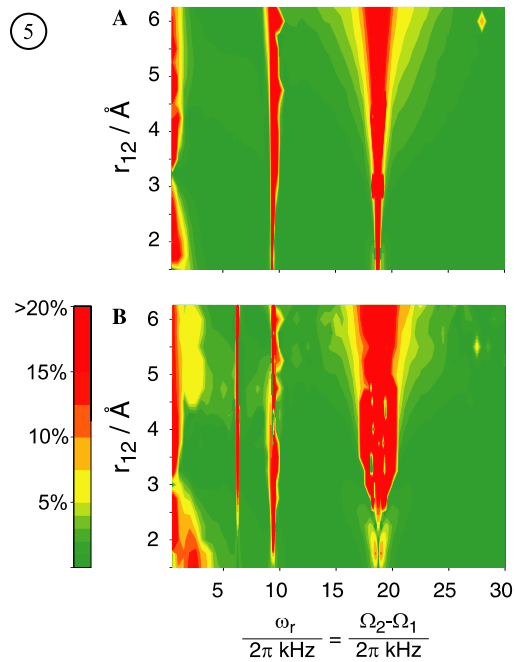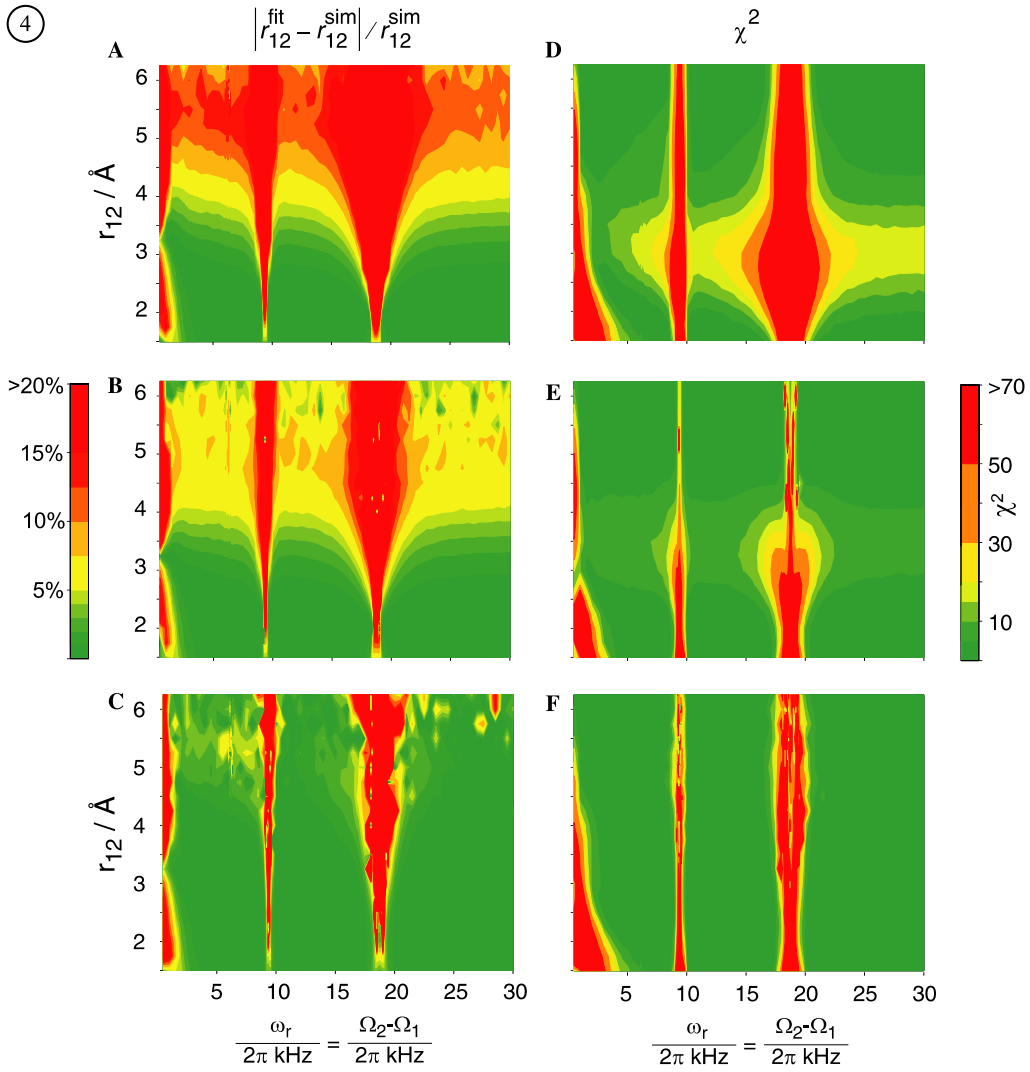
$$\left| r_{12}^{\text{fit}} - r_{12}^{\text{sim}} \right| / r_{12}^{\text{sim}}$$

$$\chi^2$$

$$\frac{\omega_r}{2\pi \text{ kHz}} = \frac{\Omega_2 - \Omega_1}{2\pi \text{ kHz}}$$

Table 2
Results from the fits on acetylcholine perchlorate

		X-ray data	Model C[a]			Model B[a]		
			Sample a	Samples b/c	Sample d	Sample a	Samples b/c	Sample d
C_1–C_3	r (Å)	3.69	3.690(16)	3.889(24)	3.84(4)	3.671(14)	3.55(3)	3.43(7)
	T_{2ZQ} (ms)		8.1	9.8	6.3	7.5	4.6	2.0
	$\Delta/2\pi$ (Hz)		9.5	34.8	40.8	[0]	[0]	[0]
	$S(\infty)$		[0.09]	[0.09]	[0.09]	0.10	0.32	0.25
C_1–C_4	r (Å)	4.73		4.55(7)	4.60(10)		4.13(11)	3.9(3)
	T_{2ZQ} (ms)			6.3	5.6		2.5	1.2
	$\Delta/2\pi$ (Hz)			31.9	42.6		[0]	[0]
	$S(\infty)$			[0.09]	[0.09]		0.28	0.32
C_2–C_3	r (Å)	2.37		2.383(3)	2.388(4)		2.378(3)	2.371(3)
	T_{2ZQ} (ms)			15.0	10.9		17.5	16.7
	$\Delta/2\pi$ (Hz)			22.0	42.7		[0]	[0]
	$S(\infty)$			[0.09]	[0.09]		0.12	0.18
C_2–C_4	r (Å)	3.63		3.643(15)	3.740(20)		3.476(16)	3.42(3)
	T_{2ZQ} (ms)			10.6	10.6		7.9	5.3
	$\Delta/2\pi$ (Hz)			30.1	39.0		[0]	[0]
	$S(\infty)$			[0.09]	[0.09]		0.26	0.35

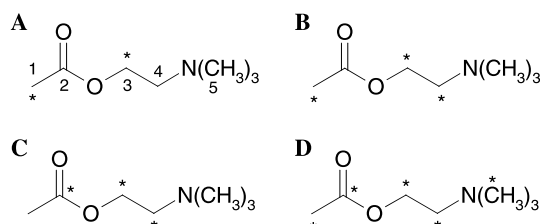[a] Values in [ ] were kept constant and fixed in the fits.

Fig. 6. The labelling schemes of the acetylcholine perchlorate samples used in the acquisition of the experimental RR curves.

five-spin systems, respectively. The compounds used in this study were synthesized as described in Appendix C and diluted to 10% in natural-abundance material. The labelling schemes are shown in Fig. 6. The chemical shifts of the five carbon atoms were determined as 19.4, 171.7, 58.8, 64.2, and 53.6 ppm for C_1–C_5. All experiments were performed at the nominal $n = 1$ RR condition for the active spin pair on a Bruker Avance 600 spectrometer equipped with a Bruker 2.5 mm MAS probe. The spinning frequency was stabilized to about ±5 Hz. Rotational-resonance experiments were performed following adiabatic cross polarization from protons [11]. After cross polarization, the polarization of one of the ^{13}C resonances was selectively inverted using a DANTE pulse train [12] empirically optimized for each of the transfer curves. After a variable mixing time, the polarization was converted to single-quantum coherence by a 90° pulse and detected. During the mixing time and data acquisition, TPPM [13] decoupling was applied using an RF-field strength of about 120 kHz, a 10° phase angle, and a pulse length of 5 μs. Each point of the polarization-transfer curve was the result of the summation of 128 transients. The data were processed and integrated into Felix 97.0 (Accelrys, CA).

The experimental transfer curves are shown in dark blue in Fig. 7, the fitted curves using model C in red. The resulting fit parameters are given in Table 2. Overall, good agreement between the different measurements as well as with the X-ray structure is observed.

It is illustrating to compare the three transfer curves between C_1 and C_3 measured in almost isolated two-spin, three-spin, and five-spin systems. Experimentally we observe that the presence of the additional passive spins causes a damping of the oscillations and slightly increases the oscillation frequency. Despite the obvious differences between the three transfer curves, the internuclear distances obtained with model C, namely 3.69, 3.88, and 3.84 Å, do not deviate from each other by more than about 5%. As expected, the result from the RR experiment on an isolated two-spin system is very close to the X-ray distance of 3.69 Å [14]. Model B yields distances of 3.67, 3.55, and 3.43 Å, respectively and underestimates the distances measured in multi-spin systems somewhat because the faster oscillation frequency is interpreted in terms of a stronger dipolar coupling only (see Eq. (24) with $\Delta_{12} = 0$). Using model B, the maximum error in the distance amounts to about 8%.

For the longest distance measured in acetylcholine perchlorate, namely C_1–C_4 with a distance of 4.73 Å, an error of less than 4% was encountered by analyzing the multi-spin RR experiments with model C, which clearly performs much better than model B which shows an error of about 20%. Additional simulations (not shown) indicate that the systematic deviations between measured and modelled curves in Fig. 7 which occur at longer mixing times even for the isolated two-spin system, should be attributed to the effect of the chemical-shielding anisotropy which is not accounted for in the
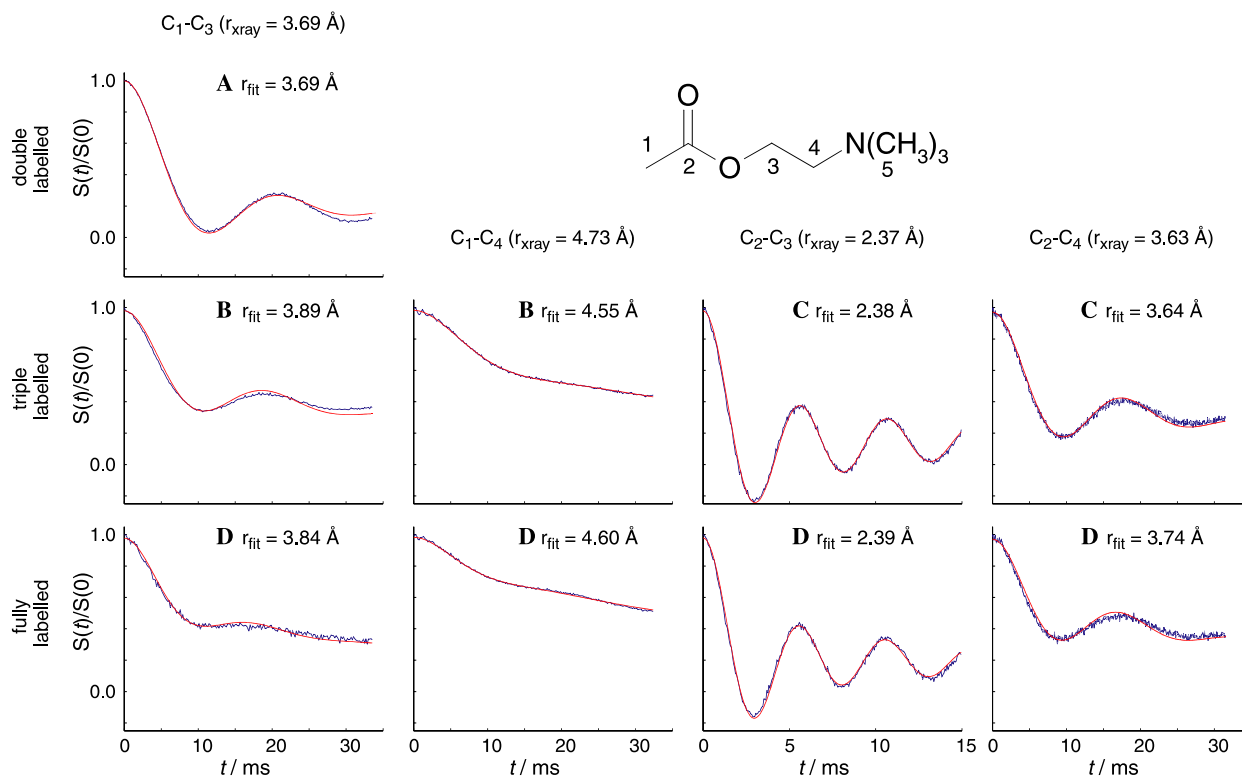
Fig. 7. Experimental RR polarization-transfer curves for acetylcholine perchlorate with labelling schemes as indicated by model C. The parameter values obtained by the fits are collected in Table 2.

model. Finally, we note that, on careful inspections of the initial behaviour of some experimental polarization-transfer curves (e.g., for the C_2–C_4 curve), the appearance of fast oscillations, as discussed in the context of the simulated data in Fig. 2D can be observed.

6. Conclusions

An improved but still very simple model is introduced which allows the evaluation of internuclear distances from multiply labelled compounds by rotational-resonance experiments obviating the need to synthesize a large number of doubly labelled compounds. The model describes the oscillation of the difference polarization between the two active spins by an effective two-spin system with a dipolar-coupling constant b_{12}^n (the parameter one is usually interested in), an effective offset $\bar{\Delta}$ from the nominal RR condition, and a zero-quantum relaxation-rate constant R_2. The parameters of the additional passive spins need not be known except that the isotropic chemical shifts should be checked to make sure that the offset of each passive spin from the nearest rotational-resonance condition is larger than the dipolar coupling to that spin. If such an undesired resonance appears, it will, however, become often apparent through the failure of the proposed models to describe the polarization-transfer curves accurately.

Our experimental data on acetylcholine perchlorate show, in agreement with numerical simulations, that it is possible to determine internuclear distances of up to about 5 Å with an accuracy better than 5% using rotational-resonance measurements in many uniformly labeled samples. The experimental data on acetylcholine, a neurotransmitter, suggest that measurements on a single sample with acetylcholine bound to the receptor, can provide information about the structure of a small molecule in the bound state. Similar experiments with other drugs or hormones are conceivable. We also foresee that the method is applicable to macromolecules because spectral crowding does, by itself, not compromise the power of the analysis presented here as only passive spins with a sizeable coupling need to be taken into account in the analysis.

While more complex models which take into account explicitly the presence of passive spins have the potential to lead to more accurate distance constraints, the model presented here has the advantage to be very simple and not to require any previous knowledge of the spin system except for the isotropic chemical shifts of the coupled spins. This information is easily obtainable by a broadband chemical-shift correlation experiment. The accuracy of the distance constraints is not quite as precise as those obtained from selectively doubly labelled compounds, but, in our hands, much higher than constraints from broadband experiments of the driven

spin-diffusion type. Finally, it should be mentioned that the accuracy of the methods described here improves with increasing magnetic field strength. Our example describes the situation at 14.1 T.

Acknowledgments

Appendix A. Fourier components

The Fourier components for the dipolar interaction are given by

$$
b_{ij}^1 = \frac{\sqrt{2}}{16}\delta_D^{(i,j)}e^{-i\gamma_{mr}}e^{-2i(\alpha_{mr}+\gamma_{pm}^{(i,j)})} \times (\sin(\beta_{pm}^{(i,j)})\sin(\beta_{mr})
$$
$$
- 2e^{i(\alpha_{mr}+\gamma_{pm}^{(i,j)})}\cos(\beta_{pm}^{(i,j)})\cos(\beta_{mr})
$$
$$
+ e^{2i(\alpha_{mr}+\gamma_{pm}^{(i,j)})}\sin(\beta_{pm}^{(i,j)})\sin(\beta_{mr})) \times (\sin(\beta_{pm}^{(i,j)})
$$
$$
+ \cos(\beta_{mr})\sin(\beta_{pm}^{(i,j)}) + 2e^{i(\alpha_{mr}+\gamma_{pm}^{(i,j)})}\cos(\beta_{pm}^{(i,j)})
$$
$$
\times \sin(\beta_{mr}) + e^{2i(\alpha_{mr}+\gamma_{pm}^{(i,j)})}(-\sin(\beta_{pm}^{(i,j)})
$$
$$
+ \cos(\beta_{mr})\sin(\beta_{pm}^{(i,j)}))) \tag{A.1}
$$

and

$$
b_{ij}^2 = \frac{1}{32}\delta_D^{(i,j)}e^{-2i\gamma_{mr}}e^{-2i(\alpha_{mr}+\gamma_{pm}^{(i,j)})}(\sin(\beta_{pm}^{(i,j)})\cos(\beta_{mr})
$$
$$
\times \sin(\beta_{pm}^{(i,j)}) + 2e^{i(\alpha_{mr}+\gamma_{pm}^{(i,j)})}\cos(\beta_{pm}^{(i,j)})\sin(\beta_{mr})
$$
$$
+ e^{2i(\alpha_{mr}+\gamma_{pm}^{(i,j)})}(-\sin(\beta_{pm}^{(i,j)}) + \cos(\beta_{mr})
$$
$$
\times \sin(\beta_{pm}^{(i,j)})))^2 \tag{A.2}
$$

with $\delta_D^{(i,j)} = -2\mu_0\gamma_i\gamma_j\hbar/(4\pi r_{ij}^3)$ and $b_{ij}^n = (b_{ij}^{-n})^*$. The Euler angles $\beta_{pm}^{(i,j)}, \gamma_{pm}^{(i,j)}$ describe the orientation of the principal-axis system of the dipolar-coupling tensors with respect to the molecular frame which is most conveniently chosen to be the principal axis system of the dipolar tensor of the active spin pair such that $\beta_{pm}^{(1,2)} = \gamma_{pm}^{(1,2)} = 0$. The other set of Euler angles, $(\alpha_{mr}, \beta_{mr}, \gamma_{mr})$, gives the orientation of the molecular frame with respect to the rotor-fixed frame. The latter set of Euler angles will be used to perform the powder average.

Appendix B. Theoretical description of rotational resonance with higher accuracy

Here we shortly discuss an approximate analytical solutions for the diagonalization of the two 3×3 subspaces of Eqs. (12) and (13) based on the Jacobi method of matrix diagonalization [15]. These formulas have been used to calculate the blue curves in Fig. 2. One of the passive dipolar couplings was assumed to be zero

$(b_{23}^n = 0)$. We first diagonalize the 2×2 subspace of spin pair (1,3) and subsequently the 2×2 subspace of the active spin pair (1,2). The off-diagonal terms still remaining after these two Jacobi steps were neglected.

This procedure leads us to the following approximation for Eq. (14):

$$
\frac{S(t)}{S(0)} = C^{-1/2} + C^{+1/2} + A_{12}^{-1/2}\cos(\omega_{eff,12}^{-1/2}t) + A_{12}^{+1/2}
$$
$$
\times \cos(\omega_{eff,12}^{+1/2}t) + A_{13}^{-1/2}\cos(\omega_{eff,13}^{-1/2}t)
$$
$$
+ A_{13}^{+1/2}\cos(\omega_{eff,13}^{+1/2}t) + A_{23}^{-1/2}\cos(\omega_{eff,23}^{-1/2}t)
$$
$$
+ A_{23}^{+1/2}\cos(\omega_{eff,23}^{+1/2}t) \tag{B.1}
$$

with the offset is given by

$$
c^{\pm1/2} = \frac{1}{64}(P_{1+2} - 2P_3)(1 - c_{13}^{\pm1/2})(5 + 7c_{13}^{\pm1/2} + (3 + c_{13}^{\pm1/2})
$$
$$
\times ((c_{12}^{\pm1/2})^2 - (s_{12}^{\pm1/2})^2)) + \frac{P_{1-2}}{128}(37 - 12c_{13}^{\pm1/2}
$$
$$
+ 2(3 + c_{13}^{\pm1/2})((c_{12}^{\pm1/2})^2 - (s_{12}^{\pm1/2})^2)
$$
$$
+ 7((c_{12}^{\pm1/2})^2 - (s_{12}^{\pm1/2})^2)) \tag{B.2}
$$

and the amplitudes by

$$
A_{12}^{\pm1/2} = \frac{P_{1-2}}{32}(3 + c_{13}^{\pm1/2})(s_{12}^{\pm1/2})^2 + \frac{(P_{1+2} - 2P_3)}{32}
$$
$$
\times (1 - c_{13}^{\pm1/2})(3 + c_{13}^{\pm1/2})(s_{12}^{\pm1/2})^2, \tag{B.3}
$$

$$
A_{13}^{\pm1/2} = \frac{(P_{1-2} - P_{1+2} + 2P_3)}{16}(1 + c_{12}^{\pm1/2})(s_{13}^{\pm1/2})^2, \tag{B.4}
$$

$$
A_{23}^{\pm1/2} = \frac{(P_{1-2} - P_{1+2} + 2P_3)}{16}(1 - c_{12}^{\pm1/2})(S_{13}^{\pm1/2})^2. \tag{B.5}
$$

Here, P_{1+2}, P_{1-2}, and P_3 represent the initial sum and difference polarization of the active spin pair and the initial polarization on spin 3, respectively, while $c_{ij}^k = \cos(\theta_{ij}^k)$ and $s_{ij}^k = \sin(\theta_{ij}^k)$ represent the cosines and sines of the tilt of the effective field with respect to the z-axis in the fictitious spin-1/2 zero-quantum subspaces of spins i and j. They are defined by

$$
c_{13}^{\pm1/2} = \Delta_{13}^{\pm1/2}/\Omega_{eff,13}^{\pm1/2} \quad \text{and} \quad S_{13}^{\pm1/2} = |b_{13}|/\Omega_{eff,13}^{\pm1/2} \tag{B.6}
$$

for the (1,3) subspace, and by

$$
c_{12}^{\pm1/2} = \Delta_{12}^{\pm1/2}/\omega_{eff,12}^{\pm1/2} \quad \text{and}
$$
$$
S_{12}^{\pm1/2} = \left(|b_{12}|\sqrt{\tfrac{1}{2}(1 + c_{13}^{\pm1/2})}\right)/\omega_{eff,12}^{\pm1/2} \tag{B.7}
$$

for the (1,2) subspace. The effective offsets from the RR condition in the two subspaces are given by

$$
\Delta_{13}^{\pm1/2} = \frac{J_{23}}{2} \pm \delta_{13} \quad \text{and}
$$
$$
\Delta_{12}^{\pm1/2} = \left(-\frac{J_{13}}{2} + \frac{J_{23}}{4} \pm \delta_{12} \mp \frac{\delta_{13}}{2} + \frac{\Omega_{eff,13}^{\pm1/2}}{2}\right) \tag{B.8}
$$

and the effective dipolar couplings are defined by

$$\Omega_{\text{eff},13}^{\pm1/2} = \text{sgn}(\Delta_{13}^{\pm1/2})\sqrt{|b_{13}|^2 + (\Delta_{13}^{\pm1/2})^2}, \tag{B.9}$$

$$\omega_{\text{eff},12}^{\pm1/2} = \text{sgn}(\Delta_{12}^{\pm1/2})\sqrt{(\Delta_{12}^{\pm1/2})^2 + \tfrac{1}{2}|b_{12}|^2(1 + c_{13}^{\pm1/2})}, \tag{B.10}$$

$$\omega_{\text{eff},13}^{\pm1/2} = \left(\frac{\Delta_{12}^{\pm1/2}}{2} - \Omega_{\text{eff},13}^{\pm1/2} + \frac{\omega_{\text{eff},12}^{\pm1/2}}{2}\right), \tag{B.11}$$

$$\omega_{\text{eff},23}^{\pm1/2} = \left(\frac{\Delta_{12}^{\pm1/2}}{2} - \Omega_{\text{eff},13}^{\pm1/2} - \frac{\omega_{\text{eff},12}^{\pm1/2}}{2}\right). \tag{B.12}$$

Appendix C. Synthesis of ^{13}C labelled acetylcholine compounds

A strategy for the synthesis of acetylcholine perchlorate was developed which permitted the introduction of ^{13}C labels in any combination of positions from a range of commercially available ^{13}C-labelled precursors. An overview is presented in Fig. C.1. The key intermediate in the synthesis of ^{13}C labelled acetylcholine compounds was the synthesis of ^{13}C-labelled 2-aminoethanol and is illustrated in detail below for [1,2-[13]C$_2$]2-aminoethanol.

Triethylamine (40 ml) was added to a cooled stirred suspension (0 °C) of ^{13}C-labelled glycine ethylester hydrochloride (18.3 g), CH_2Cl_2 (260 ml), $MgSO_4$ (13.1 g), and benzaldehyde (14.1 g). The mixture slowly reached room temperature and stirring was continued for 24 h.
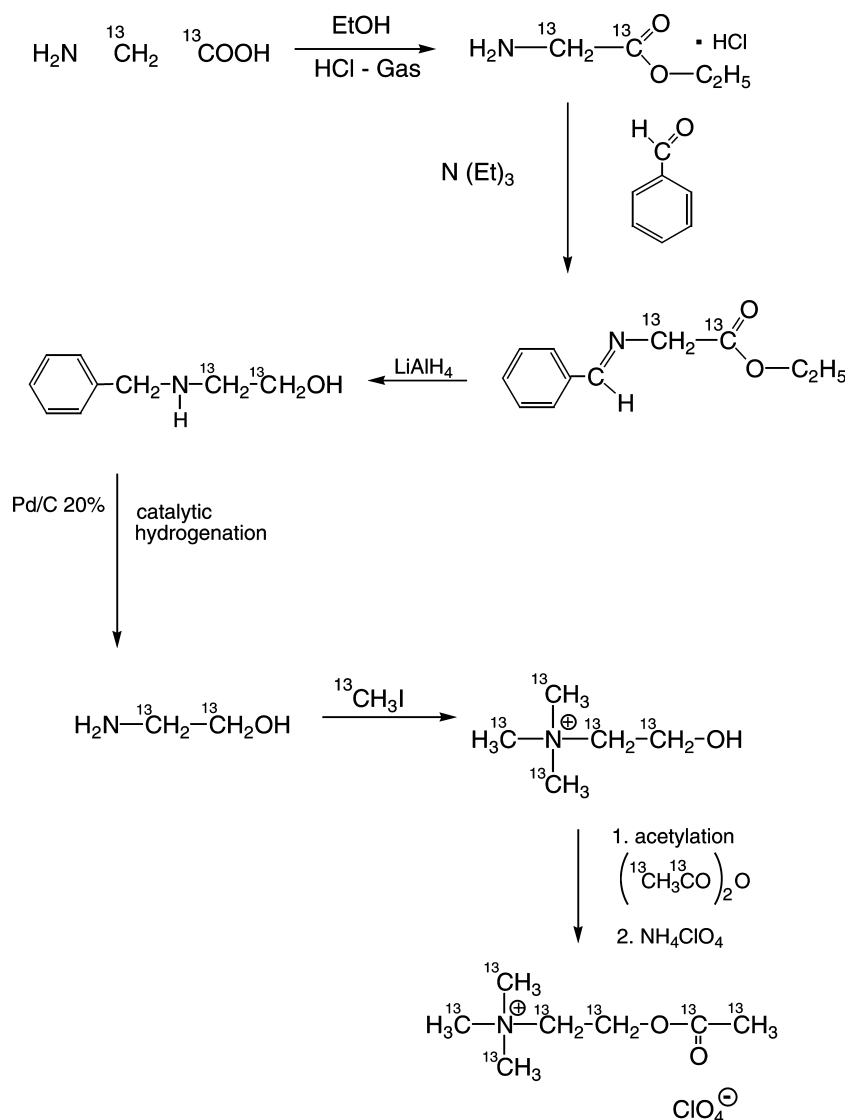

Fig. C.1. Reaction scheme for the synthesis of fully or specifically labelled acetylcholine.

The solid was filtered, the filtrate evaporated at low temperature versus a liquid nitrogen trap. The oily residue was cooled to 0 °C, diluted with water (60 ml) and extracted extensively with ether. The combined etheral extracts were dried with magnesium sulfate and again evaporated at low temperature, resulting in *N*-benzylidene-[$^{13}C_2$]glycine ethylester (25 g).

The *N*-benzylidene-[$^{13}C_2$]glycine ethylester was dissolved in dry ether (200 ml) and slowly added to $LiAlH_4$ (10 g) in ether (400 ml). After stirring at room temperature for 1 h the mixture was refluxed for 24 h. After hydrolysis with H_2O and 10% NaOH in H_2O, the suspension was filtrated. The filtrate was evaporated to yield *N*-benzylamino-[1,2-$^{13}C_2$]glycinol as a colorless oil (21 g).

The *N*-benzylamino-[1,2-$^{13}C_2$]glycinol was dissolved in CH_3OH (300 ml), Pd/C 20% (Degussa, 6 g) was added and under shaking the mixture was catalytically hydrogenated at room temperature during 20 h. The catalyst was filtered off and the filtrate was evaporated, which resulted in [1,2-$^{13}C_2$]2-aminoethanol (8.7 g).

The 2-aminoethanol was subsequently alkylated with excess methyliodide with sodium methoxide as base. The obtained choline iodide was acetylated by ^{13}C-labelled acetic anhydride in pyridine with DMAP as catalyst. The iodide counter ion was replaced by a perchlorate ion by adding the acetylcholine iodide to a saturated ammonium-perchlorate solution in water at room temperature. The compound was dissolved by heating the mixture to the boiling point. After slow cooling to room temperature, acetylcholine perchlorate crystals are obtained as needles.

References

[1] K. Wuthrich, J. Biomol. NMR 27 (2003) 13–39.
[2] For a recent review see: S. Dusold, A. Sebald, Annu. Rep. NMR Spectrosc. 41 (2000) 185–264.
[3] P.T.F. Williamson, A. Verhoeven, M. Ernst, B.H. Meier, J. Am. Chem. Soc. 125 (2003) 2718–2722.
[4] C.P. Jaroniec, B.A. Tounge, J. Herzfeld, R.G. Griffin, J. Am. Chem. Soc. 123 (2001) 3507–3519.
[5] B. Reif, R.G. Griffin, J. Magn. Reson. 160 (2003) 78–83.
[6] D.P. Raleigh, M.H. Levitt, R.G. Griffin, Chem. Phys. Lett. 146 (1988) 71–76.
[7] M.G. Colombo, B.H. Meier, R.R. Ernst, Chem. Phys. Lett. 146 (1988) 189–196.
[8] M.H. Levitt, D.P. Raleigh, F. Creuzet, R.G. Griffin, J. Chem. Phys. 92 (1990) 6347–6364.
[9] S. Smith, T. Levante, B.H. Meier, R.R. Ernst, J. Magn. Reson. Ser. A 106 (1994) 75–105.
[10] The program MINUIT was used. This is part of the PACKLIB program package and Switzerland was obtained under the conditions of the CERN Program Library/Divison CN, CERN 1211 Geneva, Switzerland.
[11] S. Hediger, B.H. Meier, R.R. Ernst, Chem. Phys. Lett. 240 (1995) 449–456.
[12] P. Caravatti, G. Bodenhausen, R.R. Ernst, J. Magn. Reson. 55 (1983) 88–103.
[13] A.E. Bennett, C.M. Rienstra, M. Auger, K.V. Lakshmi, R.G. Griffin, J. Chem. Phys. 103 (1995) 6951–6958.
[14] V. Mahajan, R.L. Sass, J. Cryst. Mol. Struct. 4 (1974) 15–21.
[15] J.C. Nash, Compact Numerical Methods for Computers, Adam Hilger, Bristol, New York, 1979.